

Journal of Photonics for Energy

SPIEDigitalLibrary.org/jpe

Strategies for light extraction from surface plasmons in organic light-emitting diodes

Jörg Frischeisen
Bert J. Scholz
Benedikt J. Arndt
Tobias D. Schmidt
Robert Gehlhaar
Chihaya Adachi
Wolfgang Brütting

Strategies for light extraction from surface plasmons in organic light-emitting diodes

Jörg Frischeisen,^a Bert J. Scholz,^a Benedikt J. Arndt,^a Tobias D. Schmidt,^a
Robert Gehlhaar,^b Chihaya Adachi,^{b,c} and Wolfgang Brütting^a

^aUniversity of Augsburg, Institute of Physics, Universitätsstraße 1, 86159 Augsburg, Germany

^bKyushu University, Center for Future Chemistry, 744 Motoooka, Nishi,
Fukuoka 819-0395, Japan

^cKyushu University, Center for Organic Photonics and Electronics Research, 744 Motoooka,
Nishi, Fukuoka 819-0395, Japan

joerg.frischeisen@physik.uni-augsburg.de

wolfgang.brueetting@physik.uni-augsburg.de

Abstract. Organic light-emitting diodes (OLEDs) usually exhibit a low light-outcoupling efficiency of only 20%. Typically, more than 30% of the available power is lost to surface plasmons (SPs). Consequently, the overall efficiency could be strongly enhanced by recovering SP losses. Therefore, three suitable techniques for extracting SPs—index coupling, prism coupling, and grating coupling—are discussed from a theoretical point of view and investigated experimentally in simplified OLED-like structures. The basic physical processes are clarified by systematic variations of the involved layer thicknesses and by excited state lifetime measurements. In addition, the analysis of the results is supported by optical simulations based on a dipole model. Finally, the advantages and disadvantages of each method, their potential efficiency for recovering SP losses, as well as the applicability in OLEDs are compared. © 2011 Society of Photo-Optical Instrumentation Engineers (SPIE). [DOI: [10.1117/1.3523314](https://doi.org/10.1117/1.3523314)]

Keywords: organic light-emitting diodes; light extraction; outcoupling efficiency; surface plasmons; gratings.

Paper 10115SSPR received Jul. 28, 2010; revised manuscript received Oct. 01, 2010; accepted for publication Oct. 04, 2010; published online Jan. 12, 2011.

1 Introduction

Since the publication of the first low-voltage organic light-emitting diode (OLED) by Tang and VanSlyke in 1987,¹ intense research has resulted in a vast number of publications and patents in the area of OLEDs, and their efficiency was continually improved due to their great potential for full color displays, backlighting, and illumination applications. However, due to the large difference in refractive index between air ($n = 1.0$), glass ($n \approx 1.5$), and organic layers ($n \approx 1.7$ to 2.0), only a small fraction of light can leave the device, resulting in a low light-outcoupling efficiency that still strongly limits the overall efficiency. In a typical OLED with optimized cavity structure, only $\sim 20\%$ of the light is emitted directly into air and roughly the same amount is trapped inside the glass substrate due to total internal reflection at the interface between glass and air.² The remaining power is lost due to the excitation of waveguide modes that propagate inside the organic layers (including the indium tin oxide electrode) or to surface Plasmons (SPs) (i.e., guided electromagnetic surface waves traveling along the interface between the organic material and the metallic cathode). In particular, excitation of SPs causes losses of typically $>30\%$ in conventional OLEDs.^{3,4}

There have been numerous suggestions in the literature to improve the outcoupling efficiency by extracting substrate modes, waveguides, and SPs.^{5,21} Probably the easiest way to get access to substrate modes is by attaching an index-matched hemispherical glass prism to the substrate, eliminating the total internal reflection at the boundary between glass and air.⁵⁻⁷ Although this method is quite efficient, it destroys the flat shape and thin structure of an OLED, which are key properties concerning their commercialization. Therefore, microstructured foils and microlens arrays have been proposed that still extract most of the substrate modes without changing the overall form factor of the OLED drastically.^{8,9}

For the extraction of waveguide modes, it was proposed to use high-index substrates that have a comparable refractive index as the organic layers. Thus, there is no total internal reflection between organic and glass and no waveguide modes are excited.^{6,7,10} Although the employment of high-index substrates is a very efficient technique, it significantly increases production costs so that it will probably not be economically advantageous for applications in general lighting.

Considering SPs, there are two basic approaches of either reducing coupling to SPs or to recover a fraction of the lost power. The easiest method to reduce coupling to SPs can be achieved by simply increasing the distance of the emitter to the cathode, because the coupling takes place via the optical near-field. The increased total thickness has the drawback that additional waveguide modes are excited, so that often only a shift of plasmon losses to waveguide losses happens without significantly increasing the overall efficiency.² A more promising approach for a strongly reduced coupling to SPs is the employment of oriented emitters that have their transition dipole moment oriented parallel to the substrate plane. In this case, the outcoupling efficiency can be enhanced by a factor of ~ 1.5 , because the coupling of horizontally oriented dipoles to SPs is significantly reduced in comparison to perpendicular dipoles. The importance of orientation has long been known for polymer OLEDs.^{11,12} Only recently was this effect also discovered in doped fluorescent organic thin films used in small molecule-based OLEDs.¹³⁻¹⁵

Concerning the recovery of SPs, there exist three basic methods. First, index coupling employs a thin cathode of a few tens of nanometers and an additional dye-doped index-coupled capping layer outside the cathode.¹⁶ Second, prism coupling also requires a thin cathode, but an additional capping layer with higher refractive index.¹⁷ Finally, grating coupling makes use of periodic surface structures in order to transform SPs into visible light. One way to achieve this is the integration of a photonic crystal inside the OLED structure.^{18,19} Another widely studied method utilizes periodic one- or two-dimensional line gratings. These gratings can be patterned into the active layers, such as the indium tin oxide anode,¹⁹ or into a polymer layer.²⁰ Alternatively, the grating can be structured into a photoresist in a preprocessing step and the OLED is built on top of this layer.²¹

In this study, we compare all three methods for recovering energy lost to SPs. Section 2 gives an overview over the basic principle of each method. In order to study the basic physical processes, we investigate simplified OLED-like structures under photoluminescence excitation. Section 3 explains the experimental setup and shows results that demonstrate each of the three techniques and prove their practicability. The advantages and disadvantages of each method as well as their potential efficiency for recovering SP losses in OLEDs are discussed.

2 Methodology

2.1 Surface Plasmon Dispersion

Surface plasmon polaritons (or simply surface plasmons) are *p*-polarized electromagnetic surface waves traveling at the interface between a dielectric medium and a metal, with maximum intensity at the interface and evanescent fields that decay exponentially into both surrounding media.^{22,23} The skin depth of the SP field in the visible wavelength regime is on the order of 100 and 25 nm for the field decaying into a typical organic material and silver, respectively.²² Figure 1(a) displays a simplified stack that is used to represent a complete OLED for studying the basic properties of SPs. An excited dye molecule in an OLED can dissipate its power either

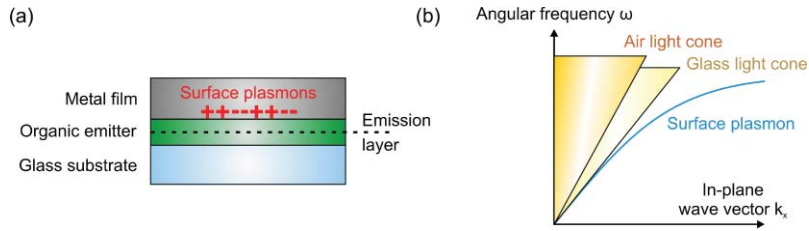


Fig. 1 (a) Simplified OLED stack. (b) Dispersion of light and SPs in the stack shown in (a).

by emitting light into air, glass, or waveguides traveling in the organic layers, or by coupling to SPs. The excitation of SPs occurs via the optical near-field of the emitting molecule, and the amount of dissipated power therefore depends on the distance to the metal. The dispersion relation of light and SPs at the planar interface between an organic layer and a metal in such a stack is shown in Fig. 1(b).

Because surface plasmons are bound to the interfacial plane, it is necessary to consider the wave vector component parallel to the interface. Therefore, the angular frequency ω is plotted versus the in-plane wave vector k_x . For propagating light, this value is defined by $k_x = k_0 \sin \theta$, with θ describing the angle of propagation with respect to the normal of the interface, and $k_0 = \omega/c$ being the vacuum wave vector with c being the speed of light. All allowed combinations of frequency and in-plane wave vectors applicable to freely propagating photons in the air half space are represented as the air light cone in Fig. 1(b). The dispersion of SPs is described by

$$k_{SP} = k_0 \sqrt{\frac{\epsilon_m \epsilon_d}{\epsilon_m + \epsilon_d}}, \quad (1)$$

where k_{SP} describes the wave vector of surface plasmons, which is per definition in the substrate plane, and ϵ_m and ϵ_d are the frequency-dependent relative permittivities of the metal and the dielectric material, respectively. Usually Ag is used as material of choice, because it has the smallest absorption loss for SPs in the visible region. Note that Eq. (1) is strictly valid only for semi-infinite layers and should be used as an approximation for thin metal films.

From Fig. 1(b), it is apparent that the wave vector of SPs is larger than the in-plane wave vector component of light for all frequencies, and no coupling between SPs and far-field radiation is possible in the case of planar interfaces. Therefore, power that is coupled to SPs by near-field coupling is dissipated as heat and therefore lost.

2.2 Index Coupling Method

The index coupling technique was proposed by Andrew and Barnes in 2004.¹⁶ The basic principle is illustrated in Fig. 2. The bottom poly(methyl methacrylate) (PMMA) layer is doped with a green dye and excited by a laser. Some power is radiated directly as light and mainly emitted into the bottom direction, but a certain fraction of power is also dissipated to SPs at the bottom

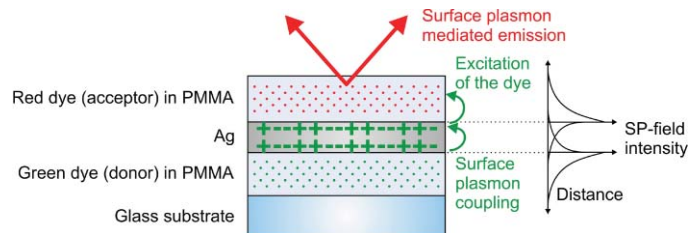


Fig. 2 Schematic drawing illustrating the index coupling method.

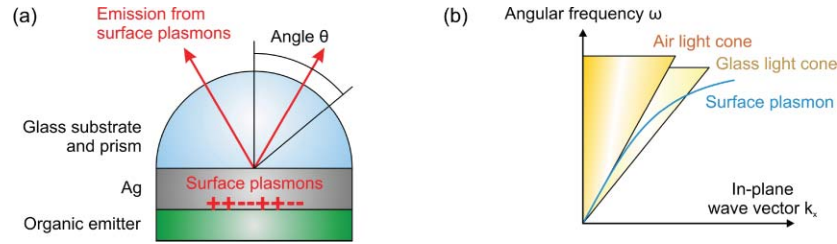


Fig. 3 (a) Illustration of the stack layout for the prism coupling technique. (b) Illustration of the air and glass light cone and schematic dispersion of SPs traveling at the interface between organic and Ag.

Ag interface via optical near-field coupling. Because there is also a PMMA capping layer on the top side of the Ag layer, the dispersion relation for SPs at both Ag interfaces is similar. Hence, SPs traveling on the bottom side may cross-couple with SPs at the top interface, and energy is exchanged between both SP modes. The upper PMMA layer is doped with a red dye whose absorption matches the emission of the green dye. Therefore, the red dye molecules can be excited by SPs, because the evanescent SP field penetrates into the PMMA layer. Altogether, some part of the energy lost to SPs by the green donor is recovered and used to excite the red acceptor dye inside the PMMA capping layer, which results in emission of red light in the top direction.

2.3 Prism Coupling Method

The prism coupling technique is based on a reversed Kretschmann configuration.^{17,22} The basic stack layout is illustrated in Fig. 3(a). The organic emitters on the bottom Ag side are excited by a laser and in turn couple to SPs at the interface between organic and Ag. If the organic layer is thin enough (i.e., only a few tens of nanometers), then the evanescent SP field penetrates through this layer into the surrounding air. Therefore, the SP dispersion in Eq. (1) is not determined by the bulk permittivity of the organic material, but by an effective permittivity of organic and air that depends on the thickness of the organic layer. Thus, it is possible that the SP dispersion lies within the glass light cone as depicted in Fig. 3(b). In the case where the Ag layer is only a few tens of nanometers thick, the SPs on the bottom side can transform into propagating light in the upper glass medium, because energy and momentum conservation between SPs and light traveling inside the glass can be fulfilled and, thus, energy lost to SPs can be recovered. By using an outcoupling prism, the light that emerges from extracted SPs can be coupled out and measured.

2.4 Grating Coupling Method

As mentioned above, another method of recovering some of the power lost to SPs is to corrugate the interface with period λ_g , as shown in Fig. 4(a). Such a submicron structure allows Bragg scattering of SPs, thus increasing or reducing the wave vector according to the relation

$$\vec{k}'_{SP} = \vec{k}_{SP} \pm m \cdot \vec{k}_g, \quad (2)$$

where \vec{k}'_{SP} describes the in-plane wave vector of the scattered SP mode, \vec{k}_g is the grating wave vector with $|\vec{k}_g| = 2\pi/\lambda_g$, and m is an integer that defines the order of the scattering process. Depending on the period of the grating and the order of scattering, it is possible to shift the SP dispersion partly into the air or glass light cone, as shown in Fig. 4(b). Hence, the energy and momentum conservation can be fulfilled for a range of frequencies and SPs are allowed to couple to far-field radiation so that some of the power lost to SPs can be recovered.

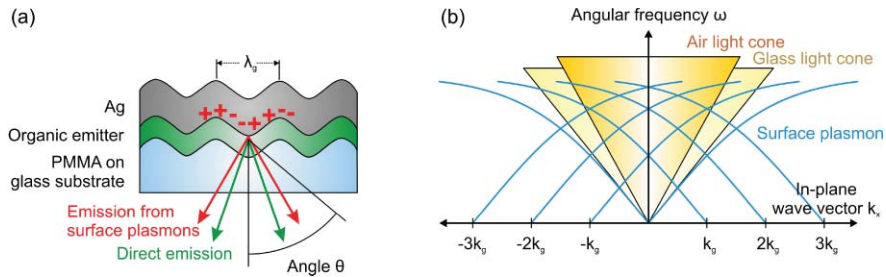


Fig. 4 (a) Illustration of the device structure used for the grating coupling method. (b) Schematic dispersion of light and SPs in a sample with periodically corrugated interfaces. Scattering of surface plasmons at the periodic grating may occur, which changes the wave vector by a multiple of the grating wave vector.

3 Experimental Results

3.1 Experimental Setup

The experimental setup and sample layouts for all coupling methods are shown in Fig. 5. Details for each sample structure and its fabrication are explained in Secs. 3.2–3.4. For the index coupling measurement in Sec. 3.2, the sample is aligned perpendicular to the collimating lens as shown in Fig. 5(a). A 375-nm cw-laser diode incident from the substrate side under 45 deg is used to excite the donor layer made of tris-(8-hydroxyquinoline)aluminum (Alq_3) doped into PMMA. Alq_3 excites SPs at the interface to Ag, and the SPs can cross-couple with the SPs on the other Ag side. There, SPs can in turn excite the red acceptor dye Lumogen Red [(LR), BASF, Ludwigshafen, Germany] doped into PMMA. No polarizer is used in this case because the emission from LR is not polarized.

For the measurement of the dispersion of directly extracted SPs in the prism and grating coupling experiment, it is necessary to measure the angular dependent emission intensity. For that purpose, the samples are mounted on a computer-controlled rotation stage, as depicted in Figs. 5(b) and 5(c). A polarizer is used in these measurements because the extracted SPs are *p*-polarized. The excitation laser is rotated together with the samples so that the excitation condition is kept constant during the measurement. The emission is measured in steps of 0.2 or 0.5 deg through appropriate long-pass filters that protect the spectrometer from the reflected laser beam.

3.2 Index Coupling Results

In order to determine the fraction of power that can be recovered by index coupling, it is necessary to use appropriate materials. Alq_3 doped at 10% wt. into a 90-nm-thick PMMA layer

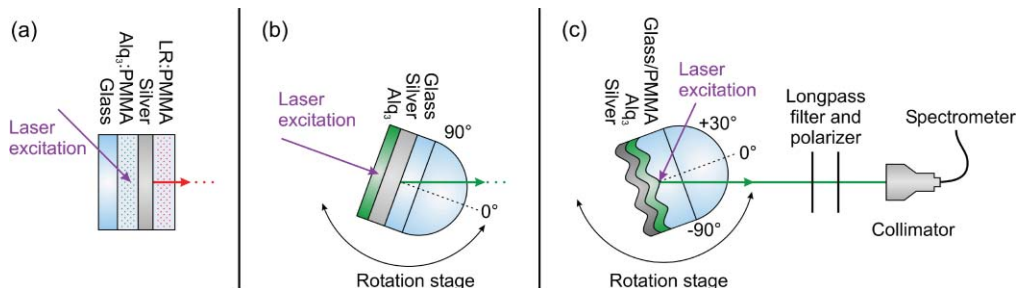


Fig. 5 Experimental setup (top view) for the measurement of (a) index coupling, (b) prism coupling, and (c) grating coupling.

(Sigma-Aldrich, Saint Louis, Missouri, $M_w = 996.000$) is used as a donor on the bottom side of a 67-nm-thick Ag layer. The acceptor layer on the top Ag side consists of Lumogen Red doped at 2% wt. into a 90-nm-thick PMMA layer. Samples were fabricated on cleaned glass microscope slides. The dye-doped PMMA layers were spin cast from a solution with 1.2% wt. PMMA dissolved in a mixture of chloroform and toluene. Alq₃ can be well dissolved in chloroform, but this solvent alone would result in a rippled PMMA surface. The Ag layers were fabricated by electron beam evaporation in a vacuum between 10^{-6} and 10^{-7} mbar. No encapsulation is required, because the bottom PMMA layer is protected by the layers above, and the upper PMMA layer only absorbs a small fraction of the incident laser beam and therefore suffers less from photodegradation.

The emission spectrum of Alq₃ fits well to the absorption spectrum of LR, which is necessary for the index coupling method. In addition, the excited state lifetime of Alq₃ is larger than that of LR, which is used to prove the energy transfer from the green donor to the red acceptor. For index coupling it is required that the SPs traveling at both Ag interfaces have a similar SP dispersion. As mentioned above, the evanescent field of the SPs decays exponentially into the surrounding media. Because glass is adjacent to PMMA on the bottom side and air on the top side, the PMMA layer must be sufficiently thick so that the SP mainly senses the PMMA without penetrating too much into glass or air. A PMMA thickness of 90 nm ensures that the SP dispersion is mainly determined by PMMA. This value corresponds to the maximum thickness before waveguide modes appear inside the upper PMMA layer. This should be avoided, because coupling of excited LR molecules to waveguide modes would reduce the desired emission from LR into air.

Besides the excitation of LR through SPs, the 375-nm cw-laser beam is partially transmitted through the Ag layer and excites the red dye directly, although the materials were chosen so that Alq₃ has a high absorption and LR has a minimum absorption at this wavelength. In addition, some emission of Alq₃ will penetrate through the Ag layer and thus emit in the top direction. For a conclusive analysis, it is necessary to distinguish between all contributions to the total emission. Therefore, three different samples are prepared for a certain silver thickness, as shown in Fig. 6(a). Sample A consists of an Alq₃-doped PMMA layer on the bottom Ag side, while the top capping layer is undoped. This sample is used to determine the fraction of Alq₃ emission that penetrates through the Ag and is measured in the top direction, as shown in the green curve in Fig. 6(b). This corresponds to the intensity that is obtained without recovery of SP losses. The doping in sample B is inverted (i.e., the bottom layer is undoped and the top PMMA layer is doped with LR). The measured intensity of this sample represents the intensity of LR emission that follows from direct excitation by the laser and is plotted as a red curve in Fig. 6(b). Finally, sample C contains two dye-doped PMMA layers on both sides of Ag. Here it is expected that additional red emission from LR occurs, which results from energy transfer from Alq₃ mediated

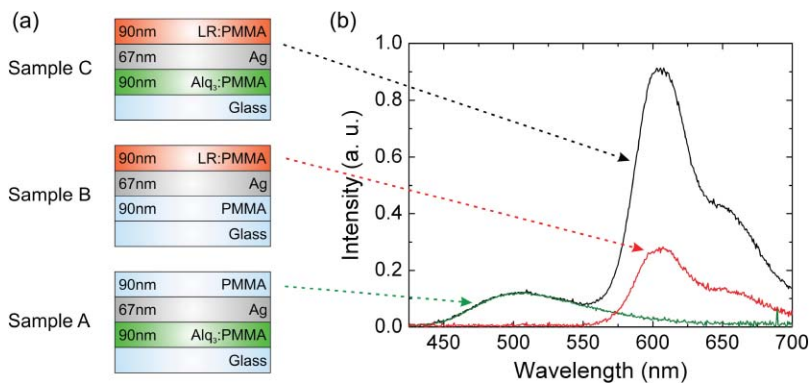


Fig. 6 (a) Overview of the sample series comprising a silver thickness of 67 nm. (b) Measured spectra in the top direction of the samples shown in (a).

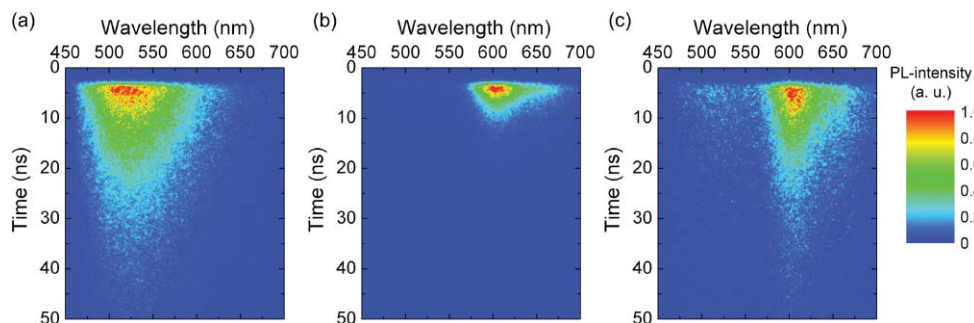


Fig. 7 Time-dependent spectral intensities for (a) sample A, (b) sample B, and (c) sample C. Samples A and B were excited and measured from the side containing the dye-doped PMMA layer, whereas sample C was excited from the donor side and the emission from the acceptor side was detected. All graphs are scaled differently in order to maximize visualization within each graph.

by SP cross-coupling. It is obvious from the black curve in Fig. 6(b) that the acceptor emission is significantly enhanced.

Integrating over the emission from each sample and subtracting the emission of samples A and B from sample C yield the amount of emission that is additionally obtained by recovering SP losses. In the case of a silver thickness of 67 nm, this additional emission is more than three times as intense as the direct emission of sample A. In other words, the emission in the top direction is increased to a fourfold intensity by recovering SP losses.

In order to verify energy transfer from Alq₃ to LR, the lifetime of the excited dye molecules is determined by a streak camera system. For that purpose, samples A to C are excited by a pulsed nitrogen laser (MNL 200, LTB Lasertechnik, Berlin GmbH, Germany, 20-Hz repetition rate and 1.2-ns pulse length) coupled with a dye in an automated tuning module so that an excitation wavelength of 375 nm similar to the cw experiments is obtained. The time-dependent spectral intensities are plotted in Figs. 7(a)–7(c). The measurements of samples A and B show the lifetime of Alq₃ and LR molecules doped into PMMA next to a 67-nm-thick silver layer, respectively, without any energy transfer effects. Obviously, the lifetime of LR is very short in comparison to Alq₃ in these samples. On the contrary, the measurement of sample C with SP mediated energy transfer shows a significantly longer lifetime in the wavelength region that corresponds to the red acceptor LR.

For a more detailed analysis, the time-dependent spectral intensities are integrated over a certain wavelength range and displayed in Fig. 8. Integrating the intensities for sample A between 460 and 660 nm and performing a monoexponential fit yields a decay lifetime of Alq₃ in PMMA of 14.8 ns. This value is very close to the result of 14.7 ns obtained by Andrew and Barnes.¹⁶ For LR in sample B, a very short lifetime of 3.3 ns is found by integrating from 565 to 700 nm and using a monoexponential fit. The decay of sample C is integrated only between 600 and 700 nm in order to ensure that the emission intensity originates from LR and not from Alq₃. The result is plotted as a black curve in Fig. 8. It is quite evident that LR does not decay with a lifetime of 3.3 ns in this case. On the contrary, the lifetime can be fitted adequately by assuming a biexponential decay with lifetimes of 3.3 and 14.8 ns. Thus, in sample C the red acceptor partially decays with a lifetime that corresponds to Alq₃. The fact that LR shows a long lifetime component in this sample can only be explained if LR is excited by the comparatively slowly decaying Alq₃. From Fig. 6(b), it can be seen that the direct emission of Alq₃ through the Ag layer is much too small in order to cause such a strong red acceptor emission. In addition, by comparing samples A and C, it can be seen that there is almost no reduction in the Alq₃ emission intensity if LR is doped into PMMA, so that the direct emission from Alq₃ cannot be responsible for the excitation of LR. Consequently, the red acceptor must be excited by SPs that in turn were excited by green donor emission. Therefore, the investigation of excited state

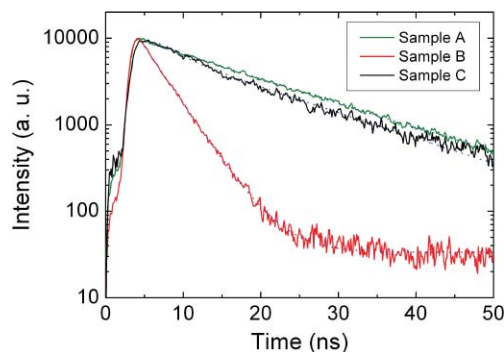


Fig. 8 Time-resolved intensity decay obtained by integrating over a certain wavelength range in Figs. 7(a)–7(c). The green curve results from integration over the measurement of sample A in Fig. 7(a) from 460 to 660 nm. The red and black curves are obtained from integration over the measurements of samples B and C in Figs. 7(b) and 7(c) from 565 to 700 nm and 600 to 700 nm, respectively. The dotted lines represent mono- or biexponential fits to the curves as described in the text.

lifetimes shows strong evidence for successful index coupling (i.e., for the SP mediated energy transfer from Alq₃ to LR through a 67-nm-thick Ag film).

The presented samples with a silver thickness of 67 nm showed that the strongest coupling among eight thicknesses varied between 28 and 96 nm. The dependence on Ag thickness basically agrees with the values obtained by Andrew and Barnes with a different stack design.¹⁶ In general, the energy transfer mediated by SPs is governed by two effects that depend conversely on the Ag thickness. First, the coupling of the green donor to SPs is enhanced with increasing thickness. Second, the transmission of the SPs through the silver is reduced with increasing Ag thickness. Altogether, there is an optimal value where the excitation of SPs from the donor is strong, but yet, a considerable fraction of SPs is able to cross-couple with SPs on the other Ag side and in turn excite the red acceptor.

Concerning the overall transfer efficiency, it should be kept in mind that the direct transmission of light through a 67-nm-thick Ag layer is very small. Thus, an increase to the fourfold intensity still corresponds to a low intensity. In order to quantify the overall efficiency, we compared the emission in the top direction to the bottom emission of Alq₃. Comparing the emission in the normal direction, it is found that despite a partial recovery of SP losses, the total top emission is a factor of ~20 smaller than the bottom emission, so that the SP mediated additional top emission amounts to only ~3% of the bottom emission. Thus, the overall efficiency of index coupling is very limited. The main reason for this is the complicated transfer process, including several steps (i.e., SP excitation by the donor, SP cross-coupling, and excitation of acceptor molecules). Each of these steps limits the overall efficiency. Above all, the red acceptor has to be positioned close to the Ag layer so that it can be excited by SPs. As a matter of fact, the excited red molecules in turn efficiently dissipate power to SPs at the Ag interface in the red wavelength range, and this power is definitely lost. The maximum efficiency obtained agrees well with the result from Tien et al., who incorporated index coupling into working OLEDs and found a maximum increase of 3% (Ref. 24). The limited efficiency is further confirmed by Celebi et al., who calculated a maximum transfer efficiency of ~6% (Ref. 25). All in all, the efficiency of index coupling seems to be insufficient for an application in OLEDs.

3.3 Prism Coupling Results

As mentioned above, it is necessary that the combination of a thin organic layer and air on the bottom Ag side provide an SP dispersion that lies within the glass light cone. Using optical simulations based on a dipole model,² the SP dispersion between a semi-infinite Ag layer and

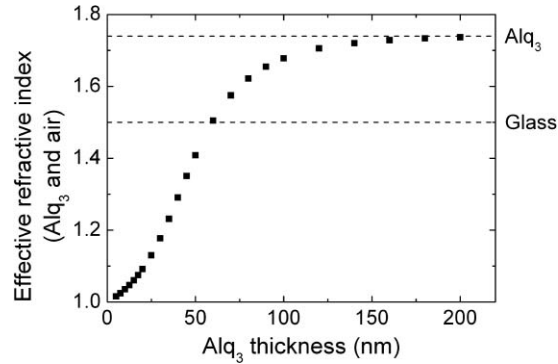


Fig. 9 Effective refractive index that determines the SP dispersion at the interface between Ag and a thin Alq₃ layer with varying thickness that is bounded by air for a wavelength of 530 nm. The dashed lines correspond to the refractive indices of glass ($n = 1.5$) and bulk Alq₃ ($n \approx 1.74$).

a thin layer of Alq₃ bounded by air can be calculated for a broad range of organic thicknesses. The simulation yields the correct in-plane wave vector of the SP dispersion. By using this value in Eq. (1), the relative permittivity ϵ_d of the thin organic layer bounded by air is obtained and an effective refractive index of organic and air can be calculated. The result is displayed in Fig. 9.

As expected, the effective refractive index has a value close to $n = 1.0$ for very small Alq₃ layers because the SPs mainly sense the air environment. For increasing Alq₃ thickness, the effective refractive index gets larger until it reaches a value of $n = 1.5$ for around 60-nm Alq₃. For larger Alq₃ thicknesses, the SP dispersion is determined by a refractive index higher than that of glass, and the Kretschmann configuration cannot be fulfilled anymore. In other words, SPs can no longer be extracted. Finally, the effective refractive index approaches the value of bulk Alq₃ if the thickness of Alq₃ is beyond ~ 150 nm, because the evanescent SP field mainly penetrates into the Alq₃ layer.

It should be noted that a semi-infinite Ag layer was used in this calculation. Using a stack with a finite Ag thickness, as shown in Fig. 3(a), results in a more complicated picture, because the emitting dipoles can also couple to a small extent to SPs traveling at the upper Ag layer, and SPs at both interfaces interact and repel each other. All in all, the condition for the Alq₃ thickness occurring in such a stack is quite similar to the result shown in Fig. 9 and, therefore, only the simple result for a semi-infinite Ag layer is presented.

The samples investigated in this section were fabricated on cleaned glass microscope slides. Silver was deposited either by thermal evaporation in a vacuum of around 2×10^{-7} mbar at a rate of 1.5 \AA/s , or by electron beam evaporation at a pressure of approximately 5×10^{-6} mbar at a rate of 1.0 \AA/s . The Alq₃ layers were fabricated by thermal evaporation in a vacuum of typically 2×10^{-7} mbar at a rate of 1.2 \AA/s . Samples with different Alq₃ and Ag thicknesses were investigated in order to determine the influence on the prism coupling process. The glass substrate was attached to a half-cylinder fused silica prism with index matching liquid in order to extract light traveling inside the glass light cone. Because extracted SPs are p -polarized, the emission intensity was measured with an appropriate polarizer. From Fig. 9 it can be seen that the SP dispersion is always determined by an effective refractive index larger than that of air. Therefore, the emission from SPs is coupled into the fused silica prism at angles clearly > 40 deg. Accordingly, all measurements are plotted from 40 to 90 deg.

In order to study the influence of the Alq₃ thickness on the SP-mediated emission, Figs. 10(a) and 10(b) show the measured SP dispersion for two samples with 50-nm Ag but with different Alq₃ thicknesses of 20 and 40 nm, respectively. It is obvious that the Alq₃ thickness determines the angular position of the extracted SPs. This agrees with the discussion about the effective refractive index of Alq₃ and air shown in Fig. 9. A larger Alq₃ thickness corresponds

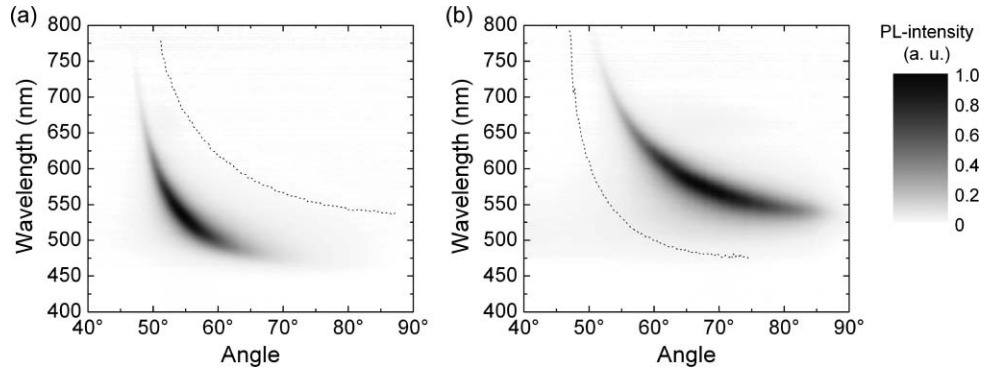


Fig. 10 Measured SP dispersion for different Alq₃ thicknesses. Both samples comprise 50-nm Ag, but have Alq₃ thicknesses of (a) 20 nm and (b) 40 nm. For better comparison, the dotted line in (a) represents the maximum intensity of the dispersion in (b), and vice versa.

to a higher effective refractive index. Consequently, the SP is located at a higher in-plane wave vector and is extracted at larger angles. If the thickness of Alq₃ gets even larger, then the SP dispersion shifts out of the glass light cone so that SPs can no longer be coupled out.

Figure 11 presents a photograph of the sample with 50-nm Ag and 20-nm Alq₃. By comparing the picture to the measurement shown in Fig. 10(a), the angular dependent SP dispersion is clearly visible. The red part of the SP dispersion is emitted at angles close to 50 deg, then the green wavelength range follows, and finally a long blue tail can be identified in the image at larger angles.

It should be noted that the absolute intensity of the measured SP dispersions in Fig. 10 is hardly influenced by the Alq₃ thickness. On the contrary, it is expected that a variation of the Ag thickness strongly influences the extracted emission intensity in analogy to the discussion in the index coupling section. The measured SP dispersion for two samples with different Ag thicknesses is shown in Fig. 12. Both samples have an Alq₃ thickness of 30 nm, but Fig. 12(a) shows a sample with 30-nm Ag, while Fig. 12(b) displays the result for a sample with a Ag thickness of 70 nm. Although the peak intensity in both graphs is quite comparable, the SP dispersion for 30-nm Ag is significantly broader. It can also be seen that the angular position in both measurements is almost similar and hence rather independent of the Ag thickness.

To investigate the influence of the Ag thickness on the transmitted SP intensity in more detail, a series of samples with eight different Ag thicknesses were fabricated and compared. For each Ag thickness, the cross section of the SP dispersion was analyzed at a wavelength of 530 nm, which is close to the emission maximum of Alq₃. Figure 13(a) shows the peak intensity

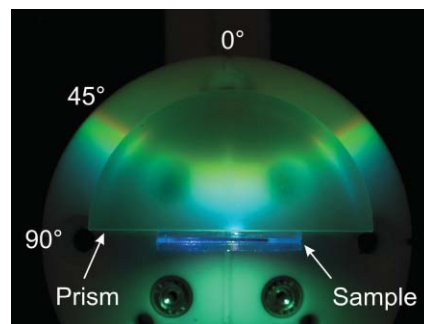


Fig. 11 Top view photograph of the sample with 50-nm Ag and 20-nm Alq₃, and attached half-cylinder prism placed on a white Teflon platform, which is attached to the rotation stage. The corresponding angular dependent measurement is shown in Fig. 10(a).

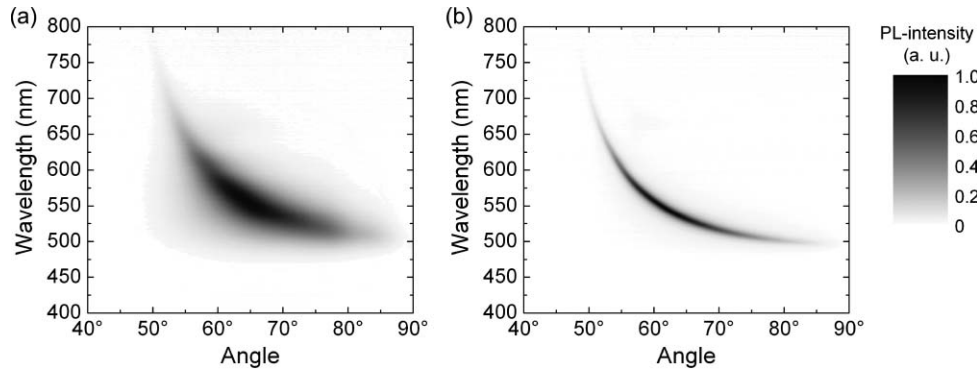


Fig. 12 Measured SP dispersion for different Ag thicknesses. Both samples comprise 30-nm Alq₃ but have Ag thicknesses of (a) 30 nm and (b) 70 nm.

of the cross sections. The highest peak emission is found at a Ag thickness of 50 nm. This result agrees perfectly with the value obtained by Winter and Barnes.¹⁷

The appearance of a maximum at a certain Ag thickness can again be explained by two competing effects. On the one hand, the amount of power coupled to SPs and the enhancement of the electric field at the metal surface increases with a larger Ag thickness. On the other hand, the SP field that transmits through the Ag layer is more attenuated with increasing Ag thickness. Winter and Barnes¹⁷ analyzed the prism-coupling method mainly in consideration for an application in biosensing. For an implementation into OLEDs, the integral intensity obtained at a certain Ag thickness should be considered instead of the peak intensity. Therefore, Fig. 13(b) displays the integral intensity from 40 to 90 deg at a wavelength of 530 nm for different Ag thicknesses. The optimum value clearly shifts to a smaller Ag thickness of ~40 nm. The reason for this is a narrowing of the extracted SP dispersion with increasing Ag thickness. This is obvious by comparing the measurements for 30- and 70-nm Ag shown in Fig. 12 and the corresponding peak and integral intensities in Fig. 13. Although the sample with 70-nm-thick Ag has a slightly higher peak intensity at 530 nm, the sample with a Ag thickness of 30 nm has a significantly larger integral intensity because the SP dispersion is much broader.

All in all, it can be concluded that the Alq₃ thickness determines the angular position of the extracted SP mode and has almost no influence on the intensity, which in turn is strongly influenced by the thickness of the Ag layer. In order to maximize the overall extracted intensity, a Ag thickness of only ~40 nm offers the best result.

Regarding the efficiency of prism coupling, it is worth comparing the method to the reversed technique of using the Kretschmann configuration to couple light through a prism into SPs. This

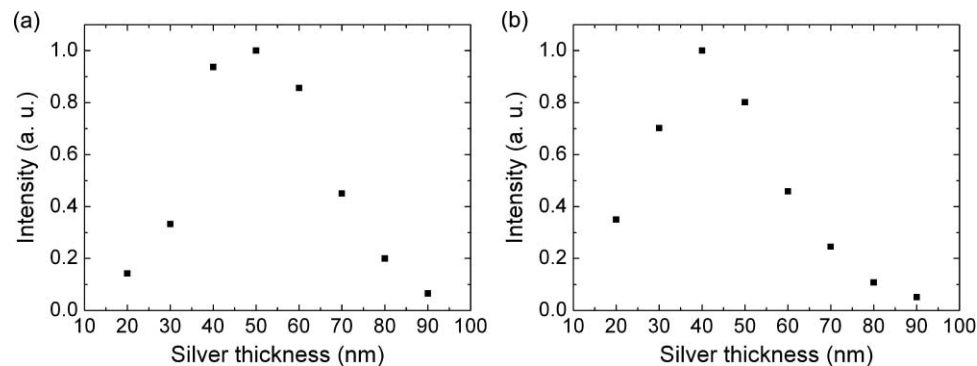


Fig. 13 (a) Measured peak intensities at a wavelength of 530 nm for different Ag thicknesses and 30-nm Alq₃. (b) Measured integral intensity from 40 to 90 deg at a wavelength of 530 nm.

is widely used in surface plasmon resonance sensors.^{26,27} In such a sensor, almost 100% of the incident light can be transformed into SPs for an optimized Ag thickness [26]. Therefore, it is expected that the prism coupling with an opposite light path investigated in this section also has a considerable efficiency of transforming SPs into propagating light. In fact, optical simulations of a stack with 40-nm Ag and 30-nm Alq₃ predict that almost 50% of the SPs on the bottom Ag side can be extracted as light into the glass prism. It should be noted that the emitting dye molecules also dissipate energy to the SPs traveling at the interface between Ag and glass. This fraction of dissipated power rapidly decreases with increasing Ag thickness, but it can be the dominating decay channel for small Ag thicknesses. Altogether, the extraction efficiency of SPs by the prism coupling method is significantly larger compared to index coupling. The main reason is that SPs are directly transformed into light in the case of prism coupling, while several intermediate steps are necessary for the index coupling technique. However, the big drawback of prism coupling is that it only works for thin organic films. For a complete OLED stack with several organic layers, the in-plane wave vector of the SPs is too large, so the SP dispersion is located outside the glass light cone and no outcoupling into the prism is possible.

3.4 Grating Coupling Results

The grating structure studied in this section was fabricated by nanoimprint lithography.²⁸ The process was carried out on cleaned microscope slides of approximately 15×15 mm². The samples were covered with PMMA (Sigma-Aldrich, Saint Louis, Missouri, $M_w = 350,000$) spin cast from a toluene solution to form a layer ~450 nm thick. Just before the imprint, the samples were heated on a hotplate to 150°C, which is above the glass transition temperature of PMMA ($T_g = 105^\circ\text{C}$). A pressure of ~50 MPa was applied for several minutes to transfer the microstructure into the PMMA layer. The mold used for the imprint process was a commercially available holographic diffractive grating (Thorlabs, Newton, New Jersey, GH13–18V) with a size of 12.7×12.7 mm² and 1800 lines/mm, corresponding to a grating period of 555 nm. No antisticking layer was used during the imprint. A 30-nm-thick Alq₃ and a 150-nm-thick Ag layer were thermally evaporated under a vacuum of around 4×10^{-7} mbar at a rate of 1.2 and 1.5 Å/s, respectively. No encapsulation was required because the thick Ag layer protects the organic from water and oxygen. In the experiment, the grating is oriented perpendicular to the plane of incidence so that SPs traveling parallel to the plane of incidence can scatter at the periodic corrugation and thus transform into propagating light. From Fig. 4(b), it is obvious that scattered SPs with a specific frequency have fixed wave vectors. In other words, the scattered SPs will be extracted at a certain angle that depends on the wavelength of the SP. Thus, it is expected that extracted SPs will show a strong angular dispersion in the measurement.

Figure 14(a) shows an atomic force microscopy (AFM) image of the periodic grating structure obtained after imprint into PMMA. The cross section presented in Fig. 14(b) illustrates the profile of the grating with an amplitude of up to 30 nm. The grating period deduced from the cross section is ~535 nm, which is close to the expected value of 555 nm based on the manufacturer information.

The measured *p*-polarized emission of the device is presented in Fig. 15(a). Besides a small background of directly emitted light, there are several strongly dispersive features that result from scattered SPs that are transformed into visible light. It should be noted that there is no SP extraction observable if the grating is rotated by 90 deg so that it is parallel to the plane of incidence. Therefore, at least a two-dimensional grating is required for the extraction of SPs traveling in different directions.

The lines in Fig. 15 correspond to the SP dispersion that was obtained from an optical simulation and shifted by a multiple of the wave vector of a grating with a period of 555 nm according to Eq. (2). The measured and simulated angular positions of the scattered SPs agree very well. The emission intensity at 0 deg (i.e., the normal direction) is determined by second-order scattered SPs, and it is maximal around a wavelength of 520 nm, where the branches of

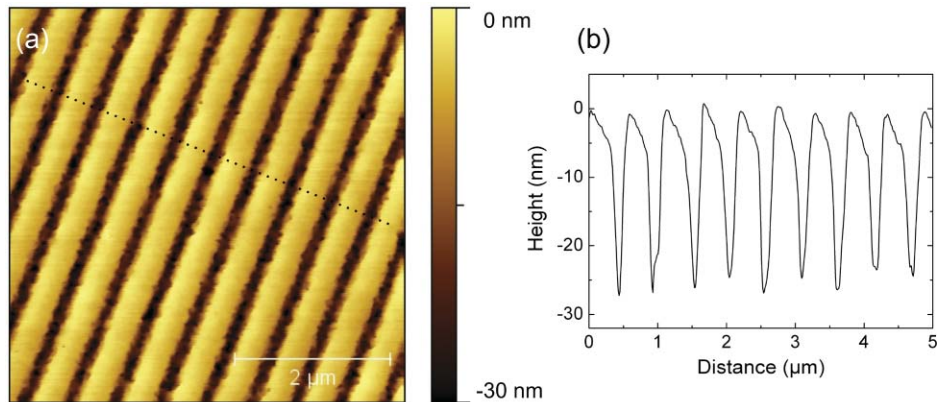


Fig. 14 (a) AFM image of the structure obtained by imprint of a grating with 555-nm period into PMMA. (b) Profile at the position indicated by the dotted line in (a).

two scattered SPs traveling in opposite directions cross each other. First-order scattered SPs lie within the air light cone at larger angles. In order to extract SPs in the green wavelength range into the normal direction by first-order scattering, a grating period of ~ 300 nm would be required.

Figure 15(b) shows a measurement of the same sample with outcoupling enhancement. For this purpose, a fused silica half-cylinder prism was attached to the glass substrate with index matching liquid. Thus, the total internal reflection at the interface between glass and air is avoided, and it is possible to extract all scattered modes within the glass light cone. Consequently, the same scattered mode in Fig. 15(b) is located at smaller angles compared to Fig. 15(a). In addition, it can be seen that the first-order scattered mode has a higher intensity and can be also extracted for shorter wavelengths. However, the integral intensity of all extracted modes is not significantly changed by applying an outcoupling prism to this sample. Thus, most of the scattered SPs can be extracted without using an outcoupling enhancement. This makes the grating coupling method especially well suited for applications in flat, large-area OLEDs, although additional scattering layers or scattering foils are necessary to turn the strong angular dispersive SP emission into isotropic light.

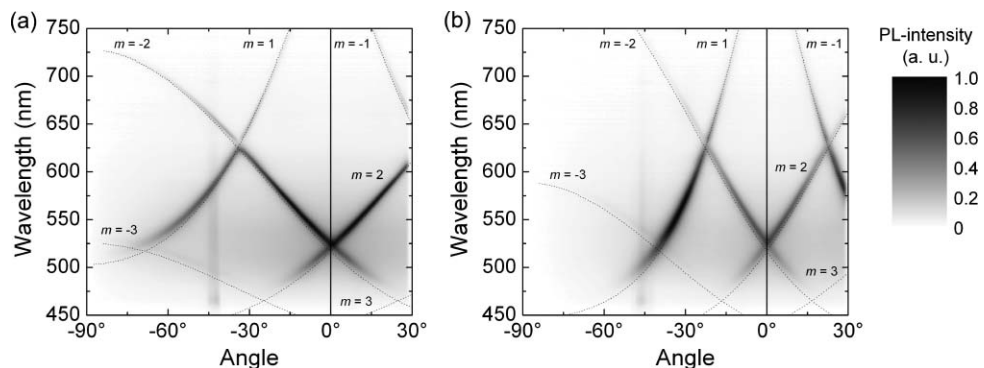


Fig. 15 (a) Measurement of the p -polarized emission. Zero degree corresponds to the surface normal in the bottom direction. The lines represent the dispersion of the surface plasmon obtained from an optical simulation and shifted by a multiple m of the wave vector of a 555-nm grating. Negative values of m denote scattering of surface plasmons traveling in the positive k_x direction and vice versa. The higher emission around -45 deg results from reflections of the incident laser beam. (b) Measurement with attached fused silica half-cylinder prism to additionally extract SPs inside the glass light cone.

The efficiency of converting SPs into light was reported to be as high as 80% using holographic gratings with optimized amplitude.²⁹ Therefore, grating coupling is probably the most promising of the three discussed methods for recovering SP losses in OLEDs. It is also noteworthy that grating coupling is the only method that extracts SPs in the bottom direction (i.e., in the same direction as the directly emitted light). Evidently, this is required for many applications in solid state lighting when the OLED is mounted to a wall or on the ceiling.

However, it should be noted that grating coupling causes a strongly dispersive emission that usually is undesired. Possible measures to solve this issue include the employment of an additional layer that contains scattering particles or converter dyes in order to make the emission isotropic again. Furthermore, gratings with a broad distribution of periods and directional randomness can enhance light extraction without introducing strongly dispersive emission. An example of such a structure is represented by spontaneously formed buckles after depositing and cooling a thin metallic film, as reported by Koo et al.³⁰

Finally, it should be mentioned that it is possible to combine index coupling and grating coupling to improve the extraction efficiency of the SP modes, as was demonstrated by Wedge et al. for top-emitting OLEDs.³¹ The grating can support the coupling of SPs to the index coupled layer, especially if the grating is corrugated only on one interface while the other is planar. By incorporating a suitable dye into the index coupled layer, it is even possible to obtain a rather Lambertian emission instead of sharp modes at certain wavelengths and directions.

4 Conclusion

In conclusion, three techniques for recovering surface plasmon losses are explained theoretically and investigated experimentally in detail. In the case of index coupling, the SP-mediated energy transfer from a donor to an acceptor is verified by lifetime studies. Although this is the only technique that provides a nondispersive emission of the recycled power, the SP extraction efficiency in this method is strongly limited and rather unsuitable for an implementation in OLEDs. For the prism-coupling technique, the influence of the thickness of organic and metallic layers on the coupling process is clarified. It should be emphasized that the metal thickness for maximum integral emission is smaller than the value required for the highest peak emission. Although the extraction efficiency in this technique is high, the application is limited to thin organic layers and thus inappropriate for an application in OLEDs. Finally, SPs are extracted by using a periodically corrugated surface fabricated by a nanoimprint of a commercially available diffractive grating. The scattering order of the extracted SPs is identified by shifting the SP dispersion calculated in a planar geometry by multiples of the grating wave vector. The grating coupling technique probably is best suited for an application in OLEDs, because the extraction efficiency of SPs is high and the recovered power is coupled out in the same direction as the directly emitted light. Clearly, it would be promising to investigate SP outcoupling in real OLED devices under electroluminescence in order to study, for example, the influence of thicker organic layers and a transparent indium-tin oxide anode with higher refractive index. Keeping in mind that usually >30% of the power in typical OLEDs is dissipated to SPs, the outcoupling efficiency of OLEDs could be significantly enhanced by recovering some of these losses.

Acknowledgments

The authors acknowledge financial support by the Elite Network of Bavaria through the international graduate school Materials Science of Complex Interfaces; by the Deutsche Forschungsgemeinschaft; by the Japan Society for the Promotion of Science; by a Grant-in-Aid for the Global COE Program “Science for Future Molecular Systems” from the Ministry of Education, Culture, Sports, Science, and Technology of Japan; by the Funding Program for World-Leading Innovative Research and Development on Science and Technology; and by the German Federal Ministry of Education and Research under Contract No. FKZ 13N10474 (TOPAS 2012).

References

1. C. W. Tang and S. A. VanSlyke, "Organic electroluminescent diodes," *Appl. Phys. Lett.* **51**, 913–915 (1987).
2. S. Nowy, B. C. Krummacher, J. Frischeisen, N. A. Reinke, and W. Brütting, "Light extraction and optical loss mechanisms in organic light-emitting diodes: influence of the emitter quantum efficiency," *J. Appl. Phys.* **104**, 123109 (2008).
3. S. Nowy, J. Frischeisen, and W. Brütting, "Simulation based optimization of light-outcoupling in organic light-emitting diodes," *Proc. SPIE* **7415**, 74151C (2009).
4. L. H. Smith, J. A. E. Wasey, I. D. W. Samuel, and W. L. Barnes, "Light out-coupling efficiencies of organic light-emitting diode structures and the effect of photoluminescence quantum yield," *Adv. Funct. Mater.* **15**, 1839–1844 (2005).
5. M.-H. Lu and J. C. Sturm, "External coupling efficiency in planar organic light-emitting devices," *Appl. Phys. Lett.* **78**, 1927–1929 (2001).
6. G. Gaertner and H. Greiner, "Light extraction from OLEDs with (high) index matched glass substrates," *Proc. SPIE* **6999**, 69992T (2008).
7. S. Reineke, F. Lindner, G. Schwartz, N. Seidler, K. Walzer, B. Lüssem, and K. Leo, "White organic light-emitting diodes with fluorescent tube efficiency," *Nature* **459**, 234–238 (2009).
8. M.-K. Wei and I.-L. Su, "Method to evaluate the enhancement of luminance efficiency in planar OLED light emitting devices for microlens array," *Opt. Express* **12**, 5777–5782 (2004).
9. Y. Sun and S. R. Forrest, "Organic light emitting devices with enhanced outcoupling via microlenses fabricated by imprint lithography," *J. Appl. Phys.* **100**, 073106 (2006).
10. S. Mladenovski, K. Neyts, D. Pavicic, A. Werner, and C. Rothe, "Exceptionally efficient organic light emitting devices using high refractive index substrates," *Opt. Express* **17**, 7562–7570 (2009).
11. J.-S. Kim, P. K. H. Ho, N. C. Greenham, and R. H. Friend, "Electroluminescence emission pattern of organic light-emitting diodes: implications for device efficiency calculations," *J. Appl. Phys.* **88**, 1073–1081 (2000).
12. J. M. Ziebarth and M. D. McGehee, "A theoretical and experimental investigation of light extraction from polymer light-emitting diodes," *J. Appl. Phys.* **97**, 064502 (2005).
13. J. Frischeisen, D. Yokoyama, C. Adachi, and W. Brütting, "Determination of molecular dipole orientation in doped fluorescent organic thin films by photoluminescence measurements," *Appl. Phys. Lett.* **96**, 073302 (2010).
14. D. Yokoyama, A. Sakaguchi, M. Suzuki, and C. Adachi, "Horizontal orientation of linear-shaped organic molecules having bulky substituents in neat and doped vacuum-deposited amorphous films," *Org. Electron.* **10**, 127–137 (2009).
15. J. Frischeisen, D. Yokoyama, A. Endo, C. Adachi, and W. Brütting, "Increased light outcoupling efficiency in dye-doped small molecule organic light-emitting diodes with horizontally oriented emitters," (submitted for publication).
16. P. Andrew and W. L. Barnes, "Energy transfer across a metal film mediated by surface plasmon polaritons," *Science* **306**, 1002–1005 (2004).
17. G. Winter and W. L. Barnes, "Emission of light through thin silver films via near-field coupling to surface plasmon polaritons," *Appl. Phys. Lett.* **88**, 051109 (2006).
18. Y.-J. Lee, S.-H. Kim, J. Huh, G.-H. Kim, Y.-H. Lee, S.-H. Cho, Y.-C. Kim, and Y. R. Do, "A high-extraction-efficiency nanopatterned organic light-emitting diode," *Appl. Phys. Lett.* **82**, 3779–3781 (2003).
19. U. Geyer, J. Hauss, B. Riedel, S. Gleiss, U. Lemmer, and M. Gerken, "Large-scale patterning of indium tin oxide electrodes for guided mode extraction from organic light-emitting diodes," *J. Appl. Phys.* **104**, 093111 (2008).

20. J. M. Ziebarth, A. K. Saafir, S. Fan, and M. D. McGehee, "Extracting light from polymer light-emitting diodes using stamped Bragg gratings," *Adv. Funct. Mater.* **14**, 451–456 (2004).
21. J. M. Lupton, B. J. Matterson, I. D. W. Samuel, M. J. Jory, and W. L. Barnes, "Bragg scattering from periodically microstructured light emitting diodes," *Appl. Phys. Lett.* **77**, 3340–3342 (2000).
22. H. Raether, *Surface Plasmons on Smooth and Rough Surfaces and on Gratings*, pp. 4–13, Springer-Verlag, Berlin (1988).
23. S. A. Maier, *Plasmonics: Fundamentals and Applications*, pp. 21–52, Springer-Verlag, Berlin (2007).
24. K.-C. Tien, M.-S. Lin, Y.-H. Lin, C.-H. Tsai, M.-H. Shiu, M.-C. Wei, H.-C. Cheng, C.-L. Lin, H.-W. Lin, and C.-C. Wu, "Utilizing surface plasmon polariton mediated energy transfer for tunable double-emitting organic light-emitting devices," *Org. Electron.* **11**, 397–406 (2010).
25. K. Celebi, T. D. Heidel, and M. A. Baldo, "Simplified calculation of dipole energy transport in a multilayer stack using dyadic Green's functions," *Opt. Express* **15**, 1762–1772 (2007).
26. J. Frischeisen, C. Mayr, N. A. Reinke, S. Nowy, and W. Brütting, "Surface plasmon resonance sensor utilizing an integrated organic light emitting diode," *Opt. Express* **16**, 18426–18436 (2008).
27. J. Homola, S. S. Yee, and G. Gauglitz, "Surface plasmon resonance sensors: review," *Sens. Actuators B* **54**, 3–15 (1999).
28. S. Y. Chou, P. R. Krauss, and P. J. Renstrom, "Imprint lithography with 25-nanometer resolution," *Science* **272**, 85–87 (1996).
29. J. Moreland, A. Adams, and P. K. Hansma, "Efficiency of light emission from surface plasmons," *Phys. Rev. B* **25**, 2297–2300 (1982).
30. W. H. Koo, S. M. Jeong, F. Araoka, K. Ishikawa, S. Nishimura, T. Toyooka, and H. Takezoe, "Light extraction from organic light-emitting diodes enhanced by spontaneously formed buckles," *Nature Photon.* **4**, 222–226 (2010).
31. S. Wedge, A. Giannattasio, and W. L. Barnes, "Surface plasmon–polariton mediated emission of light from top-emitting organic light-emitting diode type structures," *Org. Electron.* **8**, 136–147 (2007).

Jörg Frischeisen studied physics at the University of Regensburg, Germany, including one year of studies in Boulder, Colorado. He received his diploma in 2006. Subsequently, he started his PhD at the Institute of Physics at the University of Augsburg. He obtained a scholarship from the Elite Network of Bavaria in the framework of the International Graduate School of Materials Science of Complex Interfaces. His main field of research covers organic light-emitting diodes with a focus on light extraction, and the role of surface plasmon polaritons and waveguide modes in OLEDs, as well as the influence of molecular orientation in doped organic thin films.

Bert J. Scholz is a graduate student in physics at the University of Augsburg, Germany. In his diploma thesis, he is working on the improvement of the light outcoupling efficiency of OLEDs, and the role of waveguide modes and surface plasmon polaritons.

Benedikt J. Arndt received his BSc in materials science from the University of Augsburg, Germany, in 2009. He is currently studying for his European MSc in advanced functional materials at the University of Augsburg, Germany, and the Grenoble Institute of Technology, France.

Tobias D. Schmidt is a PhD student at the University of Augsburg, Germany. He graduated from teaching physics and mathematics in 2008. His current research interests are degradation processes and the exciton lifetime in organic light-emitting diodes.

Robert Gehlhaar: biography and photograph not available.

Chihaya Adachi is a professor at the Center for Organic Photonics and Electronics Research (OPERA) in Kyushu University. He is the author of more than 200 journal papers. His current research interests include organic photonics and electronics. He is a member of SPIE.

Wolfgang Brütting received his PhD in physics from the University of Bayreuth, Germany, in 1995, with a study on charge transport in 1-D charge-density wave systems. He then moved to the field of organic semiconductors, where he was involved in the development of organic light-emitting devices for display applications. Since 2003, he has been a professor of experimental physics at the University of Augsburg, Germany. His research interests include physics of organic semiconductors, in particular, thin-film growth, photophysics, and electrical transport of these materials, and related electronic devices.